

Millimeter-Wave Beamforming: Antenna Array Design Choices & Characterization

White Paper

Millimeter-wave bands are of increasing interest for the satellite industry and under discussion as potential 5G spectrum. Antennas for 5G applications make use of the shorter element sizes at high frequencies to incorporate a larger count of radiating elements. These antenna arrays are essential for beamforming operations that play an important part in next generation networks.

This white paper introduces some of the fundamental theory behind beamforming antennas. In addition to these basic concepts, calculation methods for radiation patterns and a number of simulation results, as well as some real world measurement results for small linear arrays are shown. Due to the bandwidths likely to be employed in such applications, a non-standard way of graphical representation is proposed.

Note:

Please find the most up-to-date document on our homepage

<http://www.rohde-schwarz.com/appnote/1MA276>

Table of Contents

1	Introduction	1
2	Beamforming Signals	2
2.1	Phase Coherent Signal Generation.....	2
2.2	Signal Propagation	3
3	Beamforming Architectures	5
3.1	Analog Beamforming	5
3.2	Digital Beamforming.....	7
3.3	Hybrid Beamforming	8
4	Linear Array Antenna Theory	10
4.1	Theoretical Background.....	10
4.2	Design Choices	11
4.3	Application Examples	13
5	Linear Array OTA Measurement	16
5.1	Enhancing the Simulation with Measurement Data	16
5.1.1	Measurement Results for single Elements	16
5.1.2	Simulation Results based on measured single Element Patterns	17
5.2	Antenna Scan	19
5.3	Further reading	20
6	Results and Outlook	21
7	Appendix	22
7.1	MATLAB® Pattern Generation Script	22
7.1.1	Main Function	22
7.1.2	Linear Array Factor Function	24
8	References	25

1 Introduction

Current cellular 4G networks face a multitude of challenges. Soaring demand for mobile high resolution multimedia applications brings these networks ever closer to their practical limits.

5G networks are envisioned to ease the burden on the current infrastructure by offering significantly higher data rates through increased channel bandwidths. Considering the shortage of available frequencies traditionally used for mobile communications, mm-wave bands became a suitable alternative. The large bandwidth available at these frequencies helps to offer data rates that satisfy 5G demands.

However, the mobile environment at these mm-wave bands is far more complex than at the currently used frequencies. Higher propagation losses that greatly vary depending on the environment require an updated network infrastructure and new hardware concepts.

Beamforming antenna arrays will play an important role in 5G implementations since even handsets can accommodate a larger number of antenna elements at mm-wave frequencies. Aside from a higher directive gain, these antenna types offer complex beamforming capabilities. This allows to increase the capacity of cellular networks by improving the signal to interference ratio (SIR) through direct targeting of user groups. The narrow transmit beams simultaneously lower the amount of interference in the radio environment and make it possible to maintain sufficient signal power at the receiver terminal at larger distances in rural areas.

This paper gives an overview of the beamforming technology including signals, antennas and current transceiver architectures. Furthermore, simulation techniques for antenna arrays are introduced and compared to actual measurement results taken on a small array. The theoretical antenna simulation results presented herein can be reproduced using the MATLAB® scripts in Appendix 7.1. All equations presented in this paper apply to linear antenna arrays, which for the purpose of this paper are defined as an array of equally spaced, individually excitable n radiating elements placed along one axis in a coordinate system, following [1].

2 Beamforming Signals

Beamforming in general works with simple CW-signals as well as with complex modulated waveforms. Candidate waveforms for 5G are a current research topic, since many of today's implementations suffer great disadvantages at millimeter wave bands [2].

This chapter will first introduce phase coherent signal generation before giving an overview of the most important propagation characteristics of these signals.

2.1 Phase Coherent Signal Generation

An important prerequisite for every beamforming architecture is a phase coherent signal. This term means that there is a defined and stable phase relationship between all RF carriers. A fixed delta phase between the carriers, as shown in Figure 1, can be used to steer the main lobe to a desired direction.

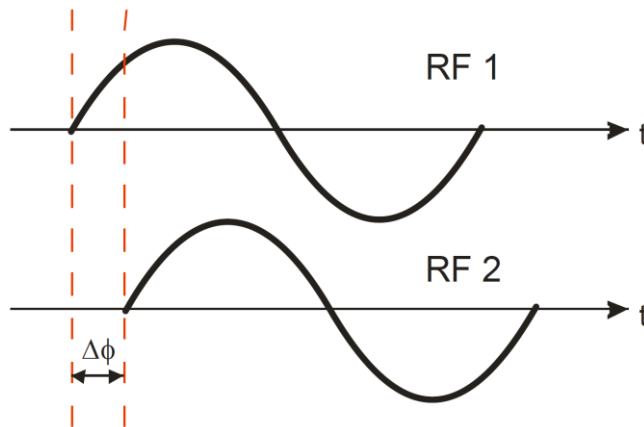


Figure 1: Phase Coherent Signals with Phase Offset

Phase coherence can be achieved by coupling multiple signal generators via a common reference (i.e. 10 MHz). A closer inspection of the instantaneous differential phase ("delta phase") of these RF signals shows instability due to:

- Phase noise of the two synthesizers
- "Weak" coupling at 10 MHz and a long synthesis chain up to the RF output
- Temperature differences which cause a change in the effective electrical length of some synthesizer components.

Because of the dominance of the second factor, the only way to stabilize the phase between two signal generators is to use a common synthesizer / LO source. This measure simultaneously eliminates the first factor [3].

Generating truly phase coherent signals using a daisy chain of signal generators is discussed in [3] and [4]. The phase coherent signals measured in chapter 5.2 were generated using a vector network analyzer.

2.2 Signal Propagation

All signals radiated from any kind of antenna share the same basic characteristics. Multipath fading and delay spread significantly reduce the capacity of a cellular network. Congestion of the available channels and co-channel interference further reduce the practical network capacity [5].

- Free Field Attenuation:** Electromagnetic waves are attenuated while travelling from the transmitter to the receiver. The free field attenuation describes the attenuation which the signal will suffer due to the distance between the two stations.

The Friis formula determines the free field attenuation:

$$P_{r,dB} = P_{t,dB} + G_{t,dB} + G_{r,dB} + 20\log_{10}\left(\frac{\lambda}{4\pi R}\right) \quad (1)$$

Where $P_{r,dB}$ is the received power level in dB, $P_{t,dB}$ the transmitted power and $G_{r,dB}$ and $G_{t,dB}$ the receive and transmit antenna gain in dBi.

Figure 2 (left) illustrates the free field attenuation over a large frequency band.

Even in case of a perfect line of sight (LoS) transmission, there are many different factors that additionally affect the magnitude of the received signal. As shown in Figure 2 (right), the resulting overall attenuation varies greatly depending on the frequency and radiation environment.

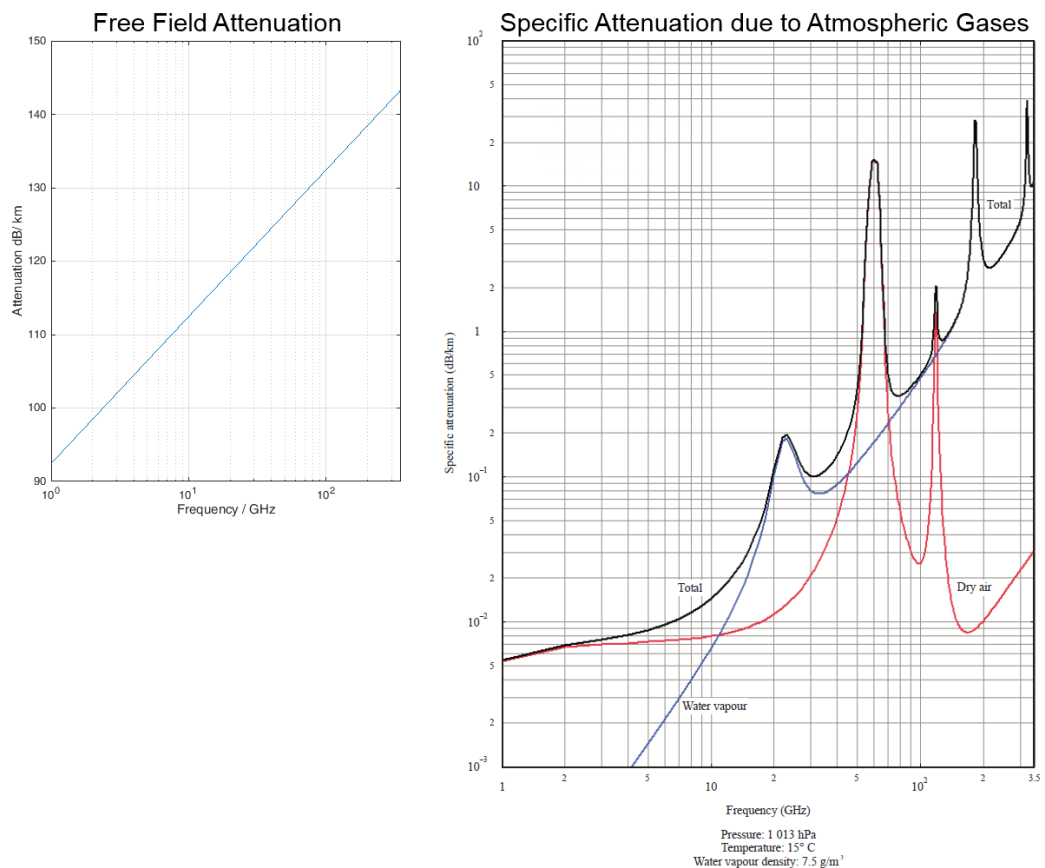


Figure 2: Free Field Attenuation approximation according to Friis Equation (left) and Attenuation due to Atmospheric Gases (right). Source: [6], pp. 16

- Fading:** The phase shift in multipath signals is non-constant due to the time variant nature of the channel. Expression (2) shows the time-dependent received multipath signal, where the complex values $a_n(t)$ and $e^{-j\theta_n(t)}$ describe the change in amplitude and phase for the transmit path n.

$$r(t) = s(t) \sum_{n=1}^N |a_n(t)| e^{-j\theta_n(t)} \quad (2)$$

The signals add up constructively or destructively depending on the current phase shift. The received signal consists of a multitude of scattered components making it a random process. Based on a sufficient amount of scattered components, this can be seen as a complex Gaussian process. This results in the creation of small fade zones in the coverage area which is called Rayleigh-Fading.

A special case of fading is the phase cancellation, which occurs when multipath signals are 180° out of phase from each other. The cancellation and thus the attenuation of the signal depends largely on the amplitude and phase balance. A 30 dB difference for example corresponds approximately to a 0.1 dB and 1.0 degree matching error.

- Delay Spread:** This effect is also due to the multipath nature of signal propagation. It describes the difference between the time of arrival of the earliest and latest significant multipath component. Typically the earliest component is the LoS transmission. In case of large delay spreads the signal will be impaired by inter-symbol interferences which dramatically increase the bit error rate (BER).

Modern beamforming antenna architectures can help to mitigate these problems by adapting to the channel. This way, delayed multipath components can be ignored or significantly reduced through beam steering. Antennas that are designed to adapt and change their radiation pattern in order to adjust to the RF environment are called active phased array antennas [5].

3 Beamforming Architectures

Millimeter-wave bands potentially enable high bandwidths. To date, the limited use of these high frequencies is a result of adverse propagation effects in particular due to obstacles in the LoS. Several transceiver architectures have been developed to compensate these issues by focusing the received or transmitted beams in a desired direction. All these solutions make use of smaller antenna element sizes due to higher carrier frequencies that enable the construction of larger antenna arrays.

Usually two variables are used for beamforming: Amplitude and phase. The combination of these two factors is used to improve side lobe suppression or steering nulls. Phase and amplitude for each antenna element n are combined in a complex weight w_n . The complex weight is then applied to the signal that is fed to the corresponding antenna.

3.1 Analog Beamforming

Figure 3 shows a basic implementation of an analog beamforming transmitter architecture. This architecture consists of only one RF chain and multiple phase shifters that feed an antenna array.

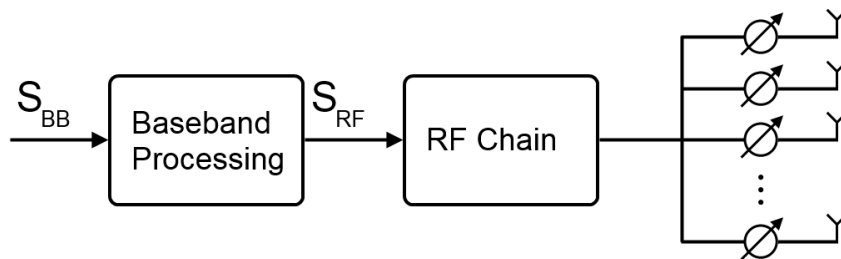


Figure 3: Analog Beamforming Architecture

The first practical analog beamforming antennas date back to 1961. The steering was carried out with a selective RF switch and fixed phase shifters [7]. The basics of this method are still used to date, albeit with advanced hardware and improved precoding algorithms. These enhancements enable separate control of the phase of each element. Unlike early, passive architectures the beam can be steered not only to discrete but virtually any angle using active beamforming antennas. True to its name, this type of beamforming is achieved in the analog domain at RF frequencies or an intermediate frequency [8].

This architecture is used today in high-end millimeter-wave systems as diverse as radar and short-range communication systems like IEEE 802.11ad. Analog beamforming architectures are not as expensive and complex as the other approaches described in this paper. On the other hand implementing a multi-stream transmission with analog beamforming is a highly complex task [9].

In order to calculate the phase weightings, a uniformly spaced linear array with element spacing d is assumed. Considering the receive scenario shown in Figure 4, the antenna array must be in the far field of the incoming signal so that the arriving wave front is approximately planar. If the signal arrives at an angle θ off the antenna boresight, the wave must travel an additional distance $d * \sin\theta$ to arrive at each successive element as

illustrated in Figure 4. This translates to an element specific delay which can be converted to a frequency dependent phase shift of the signal:

$$\Delta\varphi = \frac{2\pi d \sin\theta}{\lambda} \quad (3)$$

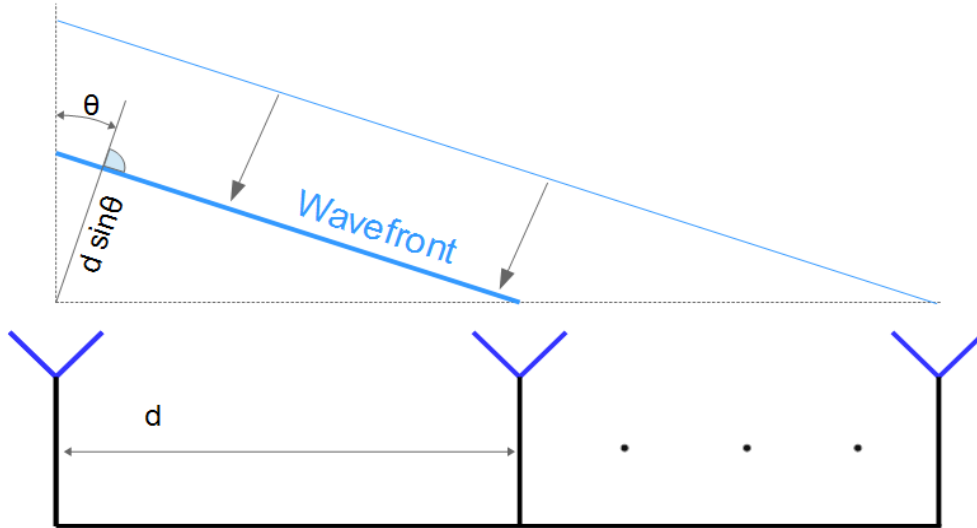


Figure 4: Additional Travel Distance when Signal arrives off Boresight [6]

The frequency dependency translates into an effect called beam squint. The main lobe of an antenna array at a defined frequency can be steered to a certain angle using phase offsets calculated with (3). If the antenna elements are now fed with a signal of a different frequency, the main lobe will veer off by a certain angle. Since the phase relations were calculated with a certain carrier frequency in mind, the actual angle of the main lobe shifts according to the current frequency. Especially radar applications with large bandwidths suffer inaccuracies due to this effect.

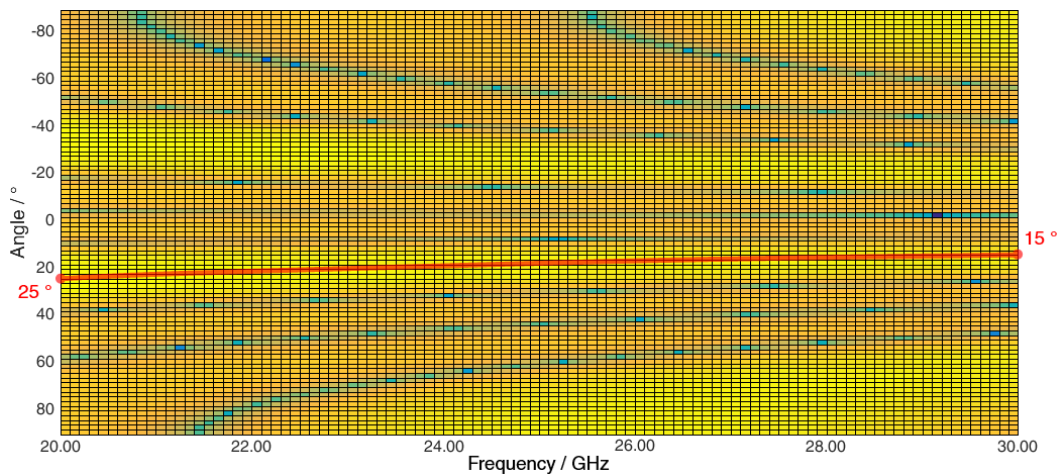


Figure 5: Simulated Beam Squint

Figure 5 shows the impact of beam squint as a function of the frequency for a linear array of four elements. The main lobe was steered to 15° at a frequency of 30 GHz. Using (3) this was achieved by a phase offset $\Delta\varphi$ of 141° per element. Due to the large bandwidth used, the beam squint effect is clearly visible at the lower frequencies, where the main lobe is located at 25°.

Expression (3) can be converted to a frequency independent term by using time delays instead of frequency offsets:

$$\Delta t = \frac{d \sin \theta}{c} \quad (4)$$

This means that the frequency dependency is eliminated if the setup is fitted with delay lines instead of phase shifters. The corresponding receiver setup is shown in Figure 6. The delay lines t_0 to t_2 compensate for the time delay Δt , which is an effect of the angle of the incident wave. As a result, the received signals should be perfectly aligned and will thus add constructively when summed up.

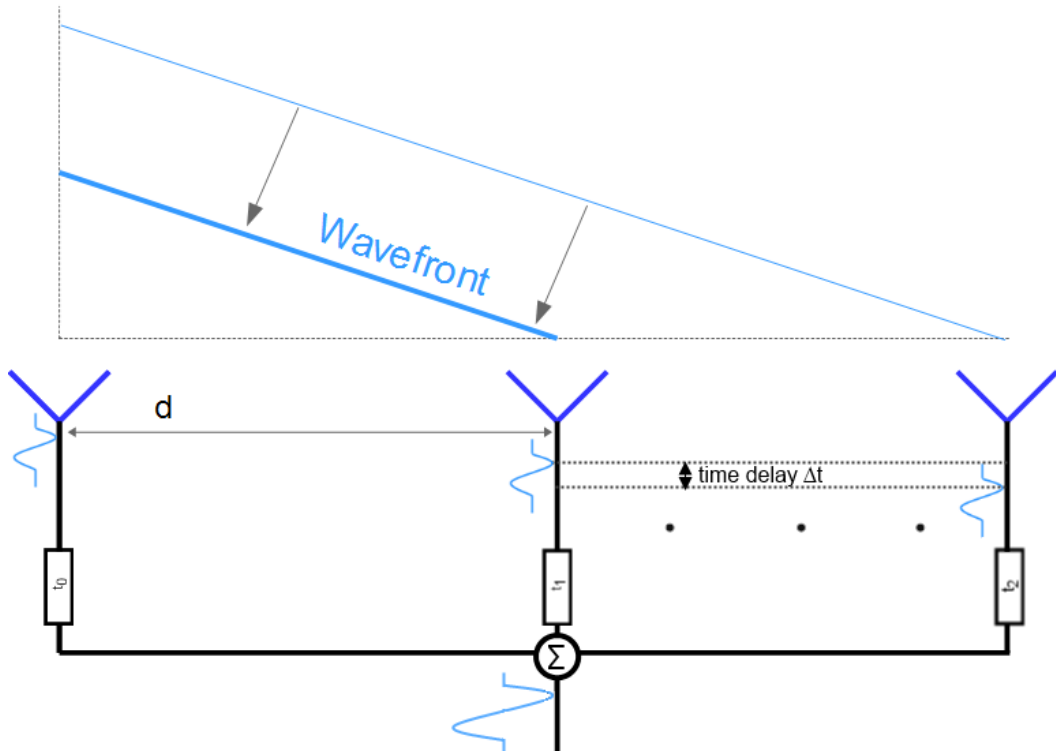


Figure 6: True Time Delay Beamsteering

The performance of the analog architecture can be further improved by additionally changing the magnitude of the signals incident to the radiators.

3.2 Digital Beamforming

While analog beamforming is generally restricted to one RF chain even when using large-number antenna arrays, digital beamforming in theory supports as many RF chains as there are antenna elements. If suitable precoding is done in the digital baseband, this yields higher flexibility regarding the transmission and reception. The additional degree of freedom can be leveraged to perform advanced techniques like multi-beam MIMO. These advantages result in the highest theoretical performance possible compared to other beamforming architectures [10].

Figure 7 illustrates the general digital beamforming transmitter architecture with multiple RF chains.

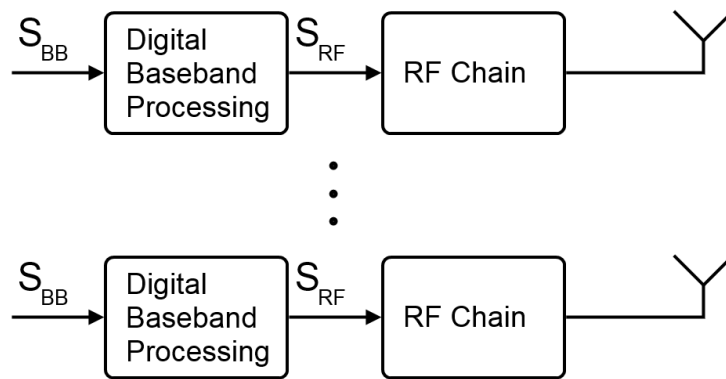


Figure 7: Digital Beamforming Architecture

Beam squint is a well-known problem for analog beamforming architectures using phase offsets. This is a serious drawback considering current 5G plans to make use of large bandwidths in the mm-wave band. Digital control of the RF chain enables optimization of the phases according to the frequency over a large band.

Nonetheless, digital beamforming may not always be ideally suited for practical implementations regarding 5G applications. The very high complexity and requirements regarding the hardware may significantly increase cost, energy consumption and complicate integration in mobile devices. Digital beamforming is better suited for use in base stations, since performance outweighs mobility in this case.

Digital beamforming can accommodate multi-stream transmission and serve multiple users simultaneously, which is a key driver of the technology.

3.3 Hybrid Beamforming

Hybrid beamforming has been proposed as a possible solution that is able to combine the advantages of both analog and digital beamforming architectures. First results from implementations featuring this architecture have been presented in prototype level, i.e. in [11].

A significant cost reduction can be achieved by reducing the number of complete RF chains. This does also lead to lower overall power consumption. Since the number of converters is significantly lower than the number of antennas, there are less degrees of freedom for digital baseband processing. Thus the number of simultaneously supported streams is reduced compared to full blown digital beamforming. The resulting performance gap is expected to be relatively low due to the specific channel characteristics in millimeter-wave bands [9].

The schematic architecture of a hybrid beamforming transmitter is shown in Figure 8. The precoding is divided between the analog and digital domains. In theory, it is possible that every amplifier is interconnected to every radiating element.

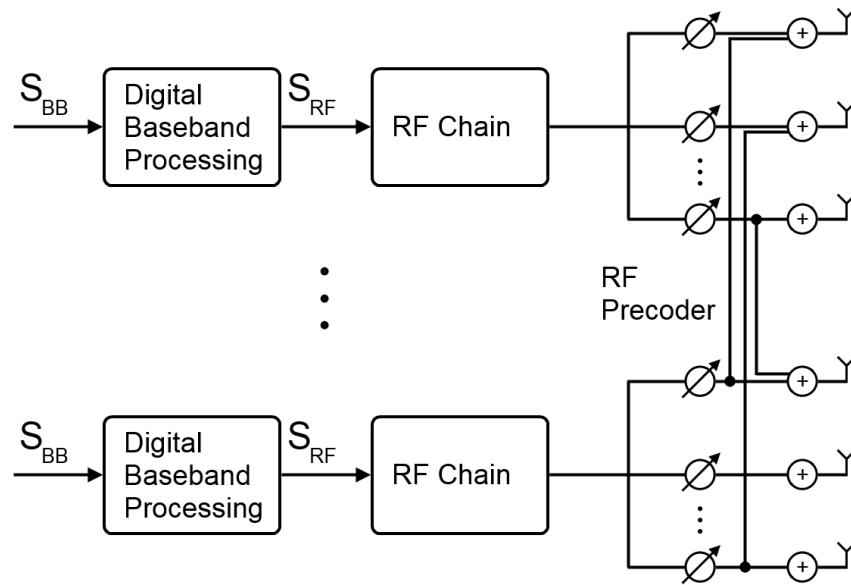


Figure 8: Hybrid Beamforming Architecture

4 Linear Array Antenna Theory

This chapter consists of two sections. The first introduces some theory while the second section demonstrates the application of these equations by using a suitably chosen visualization of the results obtained by simulating a linear antenna array of ideal, isotropic elements.

4.1 Theoretical Background

In this chapter, a linear antenna array with N equally spaced isotropic radiating elements is assumed. These elements can be imagined being placed along the x-axis of a spherical coordinate system, as shown in Figure 9. The following section introduces the theory behind the simulation of this type of antenna.

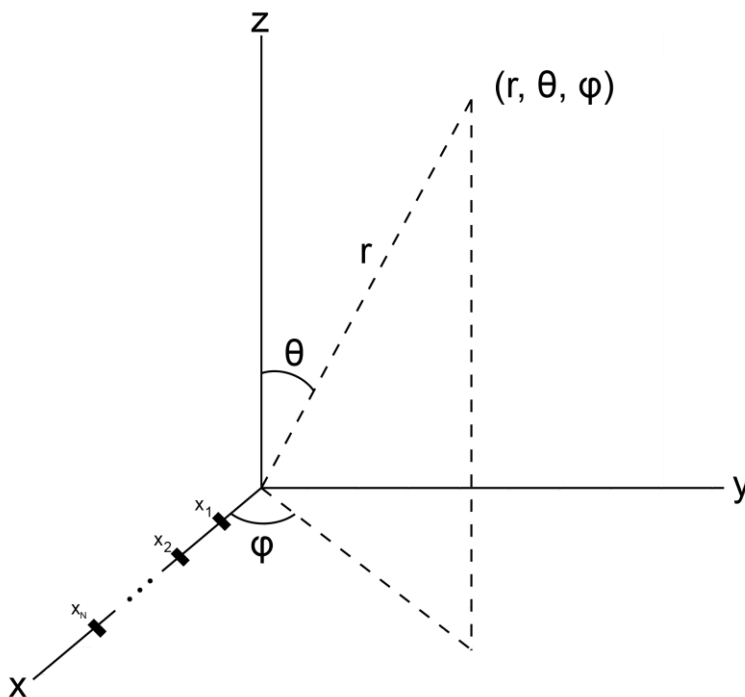


Figure 9: Linear Antenna Array

The radiation pattern F_{array} of a linear antenna array can be approximated by multiplying the array factor AF_{array} with the element radiation pattern $F_{element}$ that is considered equal for all elements assuming a large enough array [12].

$$F_{array}(\theta, \phi) = F_{element}(\theta, \phi) * AF_{array}(\theta, \phi) \quad (5)$$

If the number of antenna elements is small, the assumption of equal radiation patterns does not hold. The outer elements may deviate by a large degree from the pattern of the other antennas, which cannot be neglected in case of only a few elements. Thus (5) is only applicable for coarse approximation in this case. Mutual coupling and losses in the elements are not considered in this equation, too. These effects contribute to a modified beam pattern manifested in for example increased side lobe levels [1].

Aside from the element radiation pattern F_{element} , the array factor AF_{array} is required to calculate F_{array} according to (5). The linear array factor depends on the wavelength λ , the angle direction θ , the distance d between the elements and the number of elements N [1]:

$$AF_{\text{array}}(\theta, \phi) = \sum_{n=1}^N a_n e^{jnkd \sin\theta \sin\phi} e^{j\Delta\varphi}; k = 2 * \pi/\lambda \quad (6)$$

The complex weighting introduced in chapter 3 can be set using (6). The amplitude weights are applied per element by the factor a_n . The angle $\Delta\varphi$ calculated with the basic beam steering formula (3) can be used to steer the beam to an arbitrary angle.

Equation (6) can be simplified by introducing ψ , which describes the far-zone phase difference between adjacent elements [13].

$$\psi = kd \sin\theta \sin\phi + \Delta\varphi \quad (7)$$

Substituting (7) in equation (6) results in:

$$AF_{\text{array}}(\theta, \phi) = \sum_{n=1}^N a_n e^{jn\psi} \quad (8)$$

The series in (8) can be further simplified and normalized. This leads to the normalized array factor [13]:

$$|AF_{\text{array}}(\psi)| = \frac{1}{N} \left| \frac{\sin(N\psi/2)}{\sin(\psi/2)} \right| \quad (9)$$

The normalized array factor is periodic in 2π and allows to infer a lot of information about the characteristics of the linear antenna array, as will be shown in the next chapter.

4.2 Design Choices

This chapter focuses on the properties of the array factor introduced in the previous section and the implications for the design of beamforming antennas.

Equation (6) to (9) show that the number of elements and their equidistant spacing have a great influence on the characteristics of a linear antenna array. The effects of modifying these two parameters will be explained by the example of Figure 10.

The diagrams on the left show the normalized array factor $|AF_{\text{array}}(\psi)|$ for an antenna with an equidistant spacing of 5 mm between elements. The element distance is thus slightly smaller than 0.5λ at 28 GHz. The normalized array factor of an antenna with a spacing of 16 mm, which corresponds roughly to 1.5λ , is displayed on the right side. Diagrams on the upper half were calculated for an array of four elements, while the array factors displayed in the plots on the lower half belong to arrays consisting of 16 elements.

Comparing the upper and lower diagrams of Figure 10 illustrates the effect of increasing the number of elements while keeping the equidistant spacing constant. The main lobe width decreases for a larger element count. This means that the more elements a linear array consists of, the more directivity will be observed. Another effect of increasing the number of elements is a larger number of side lobes with an overall decrease in level.

The directivity of a linear array can also be improved by increasing the distance between elements, which produces a narrower main lobe. Similar to a larger number of elements, the number of side lobes will increase, albeit without a reduced level. On the contrary, a large inter-element gap produces side lobes that are of equal level compared to the main lobe. The red dots in Figure 10 highlight this effect for the antenna with a spacing of 1.5λ . The side lobes marked by red dots are called grating lobes. In general these grating lobes are undesired as energy will be radiated to or received from unwanted directions. In

applications that demand large bandwidths, grating lobes may only affect part of the frequencies of operation.

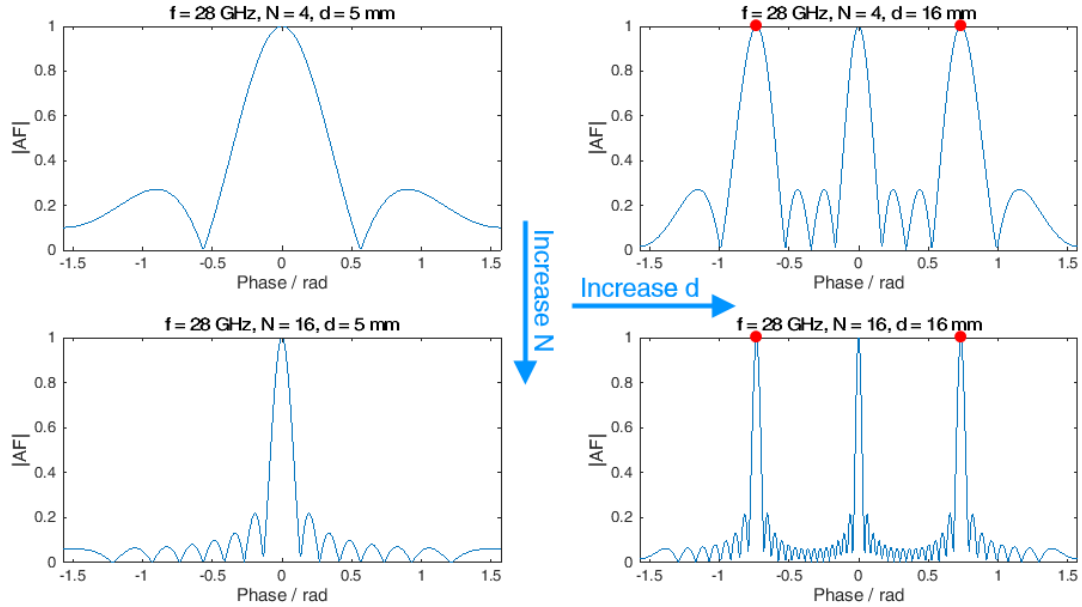


Figure 10: Normalized Array Factor for multiple Configurations

Linear arrays with equidistant element spacing will produce grating lobes if the inter-element spacing exceeds half a wavelength. In order to avoid this phenomenon from occurring in the visible region, which is defined as the range $[-90^\circ, 90^\circ]$, following condition must be kept:

$$d < \frac{\lambda}{2} \quad (11)$$

If equation (11) is violated, grating lobes of increasing level begin to appear in the visible region. In case that the distance between the elements exceeds one wavelength, the grating lobe levels start to equal the main lobe level.

Due to the periodicity of the array factor, grating lobes enter the visible region coming from the invisible region. In case of grating lobes entering the visible region, the scan angle has to be restricted or the element spacing must be decreased. The maximum scan range $|\theta_0|$ for a given element distance d is defined in the grating lobe criteria [14]:

$$\sin|\theta_0| \leq \frac{\lambda}{d} - 1 \quad (12)$$

Rearranging equation (12) helps to calculate the maximum value of d for a given scan range $|\theta_0|$:

$$\frac{d}{\lambda} < \frac{1}{1 + \sin|\theta_0|} \quad (13)$$

If a scan range of $|\theta_0| < 45^\circ$ is chosen, the element distance should not exceed 0.58λ in order to avoid grating lobes in this region.

Suppression and manipulation of grating lobes is a current research topic. It has been demonstrated that the position and levels of grating lobes can be manipulated by modifying the element shape [15]. Using non-uniform element spacing allows to suppress certain grating lobes but adds a considerable layer of complexity.

4.3 Application Examples

All radiation patterns shown in this section are simulation results that were calculated using equations (5) and (6). The scripts in appendix 7.1 can be used to generate and modify these patterns by changing the simulation parameters.

Figure 11 shows the simulation results of a radiation pattern over a frequency range from 24 to 30 GHz in 2D-swept view. This graphical representation was chosen in order to offer an improved overview of the antenna's behavior over the whole bandwidth. The assumed antenna has four isotropic elements with a free space distance of 16 mm. This geometry corresponds to the antenna used in chapter 5.

Both transmit and receive antenna are considered isotropic and the transmit power was set to 0 dBm. The distance between transmit and receive antenna was set to 2 m, which lies in the assumed far field.

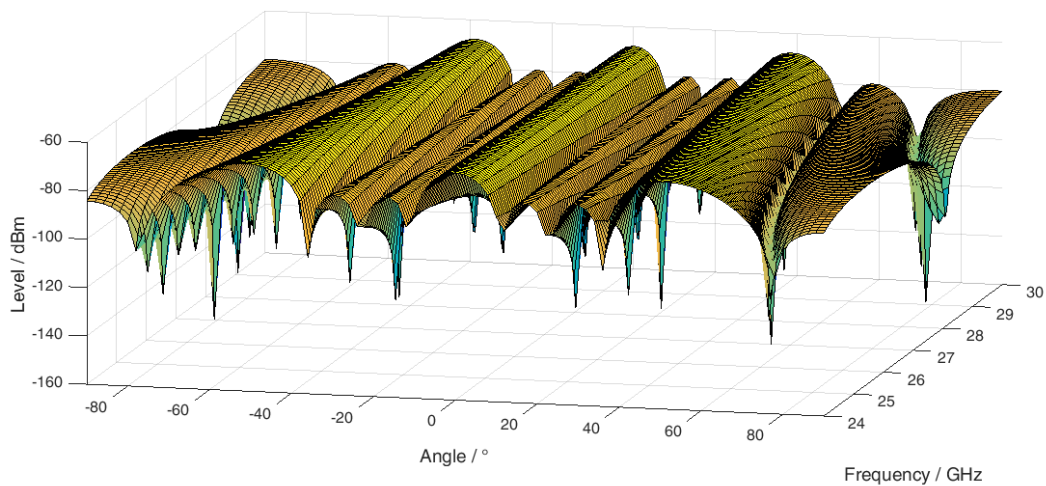


Figure 11: Simulation of a Linear Antenna Array with zero Phase Offset in 2D-swept view

The plot of Figure 11 shows occasional discrete level dropouts, i.e. observed signal level changes abruptly and significantly. These angle/frequency combinations are intrinsic to the mathematical expressions presented in the previous section. Attenuation according to Friis' formula is also included in the model.

Figure 12 demonstrates the use of expression (3) for steering the beam to an arbitrary angle. In this case, the phase offsets were calculated for 28 GHz and the antenna parameters described in the previous section. Thus, in order to steer the beam 10° to the right, a phase offset of $\Delta\varphi = 94^\circ$ was set to each element.

As would be expected using equation (12), the side lobes are located at approximately $\pm 40^\circ$. A closer look at the simulated pattern shows the high frequency dependency of this value.

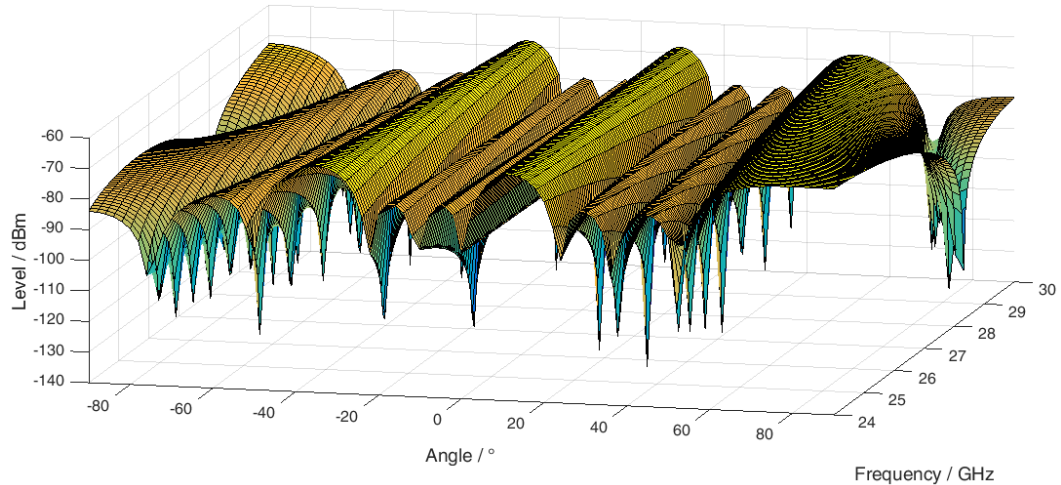


Figure 12: Simulation of a Linear Antenna Array with Phase Offset

While the phase offsets of the antenna elements are generally used to determine the angle of the main lobe, the amplitude weighting provides means to modify the beam width and side lobe levels. In case of unity amplitude weights ($[1, 1, 1, 1]$), the main beam width is smallest.

Decreasing the amplitude levels of the outside elements results in an increased main beam width. If the weights of the outside elements approach zero ($[0, 1, 1, 0]$), the radiation pattern is approximately equal to a two element array with the same dimensions. The side lobe levels are usually controlled by applying window functions. Every change of the weights leads to a change in the radiation pattern, while each window has its own set of advantages and drawbacks [16].

Figure 13 shows the previously discussed effect of different amplitude weights. While the weighting $[1, 1, 1, 1]$ was used for the simulation shown in Figure 11 and Figure 12, the weighting factor of the outer elements was reduced to 0.2 in Figure 13. Thus the resulting weight vector was $[0.2, 1, 1, 0.2]$. The increased beam width is clearly visible in a direct comparison between the figures.

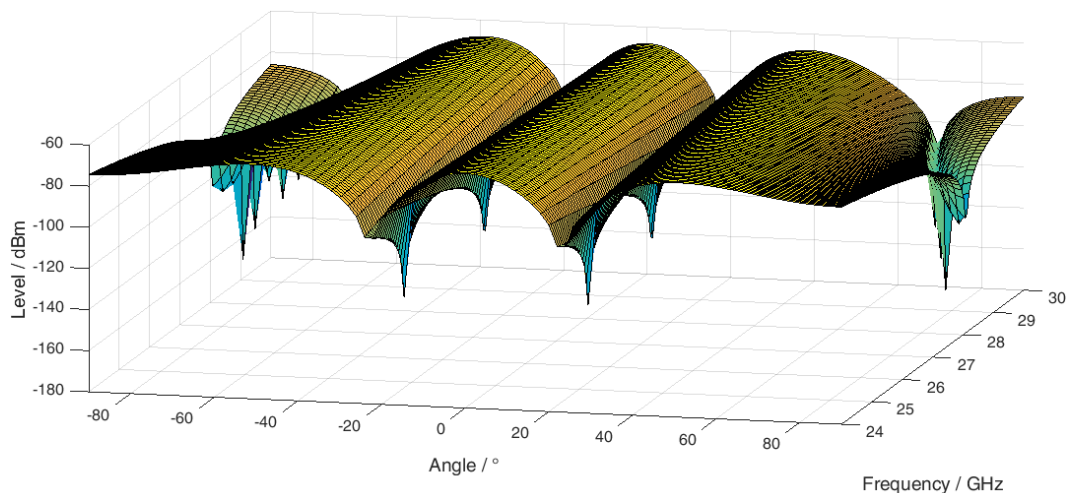


Figure 13: Simulation of a Linear Antenna Array with different amplitude weighting

Non-equal amplitude weightings are an important instrument for discriminating between two directions. A small trade-off in terms of directive gain for an intended user may result in a much larger rejection of unintended signals.

The left of Figure 14 shows the rejection of an unintended user signal at 60° assuming a signal equal to the one in Figure 11 at 28 GHz is radiated. The red square corresponds to the rejection at the position of the unintended user. The right part of Figure 14 shows the effect of unequal amplitude weightings applied to the transmitter. The rejection at the unintended user increased by approximately 23 dB

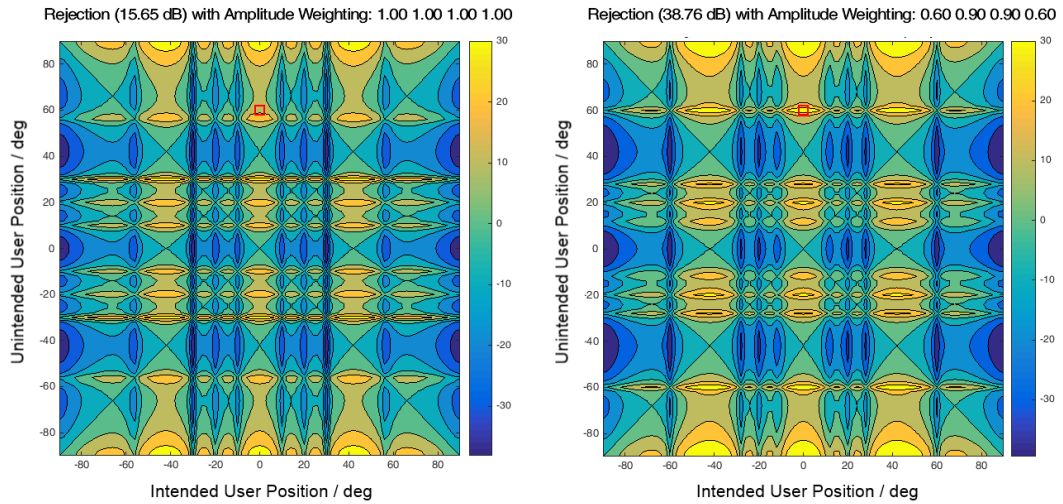


Figure 14: Increase in Interferer Rejection through non-equal Amplitude Weights at 28 GHz

5 Linear Array OTA Measurement

This chapter will first introduce the effects on the simulated array of using measured data for the element radiation pattern F_{element} . Afterwards, the actual over-the-air (OTA) measurement results obtained from an antenna scan measurement are shown in order to complement the theoretical calculations.

5.1 Enhancing the Simulation with Measurement Data

5.1.1 Measurement Results for single Elements

The antenna whose elements were measured is a linear array consisting of four elements with equidistant spacing. Figure 15 shows the superimposed, normalized radiation patterns of all elements of the antenna at 28 GHz. The measurements were conducted separately, meaning the other elements were inactive and terminated. Figure 16 shows the level of the main lobe at boresight over the whole frequency range of one element.

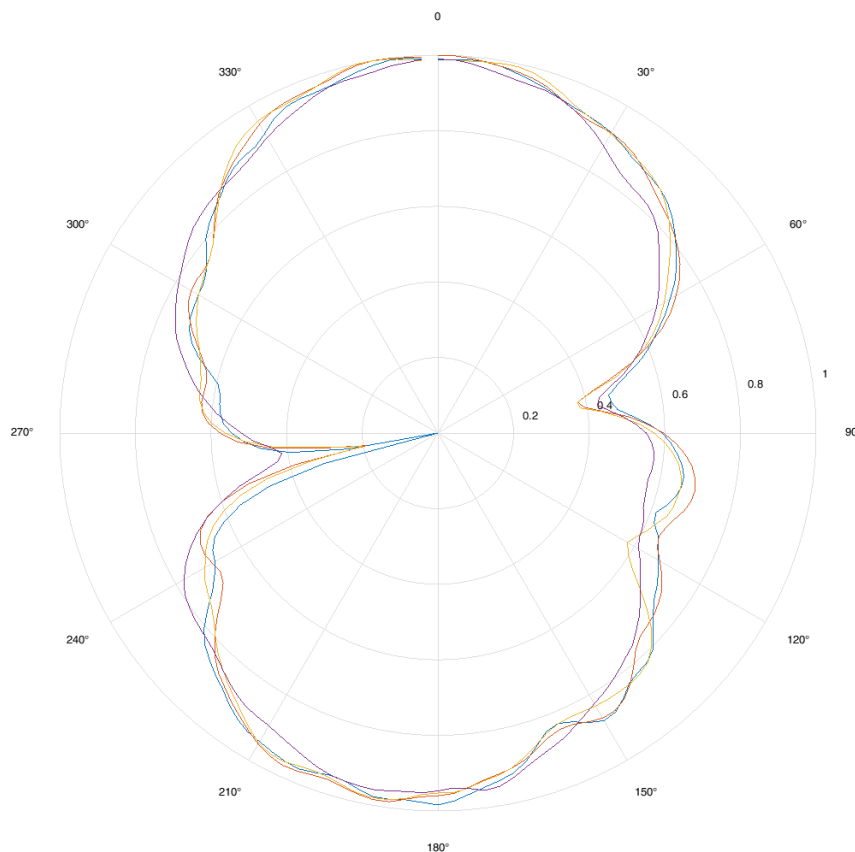


Figure 15: Antenna Element Radiation Pattern

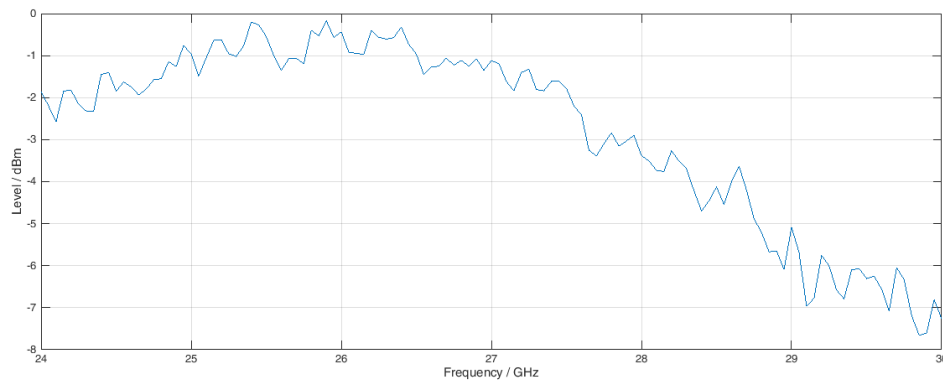


Figure 16: Boresight Level of the Main Lobe of one single Element

Figure 17 shows the swept 2D radiation pattern of one single element over the frequency range from 24 to 30 GHz.

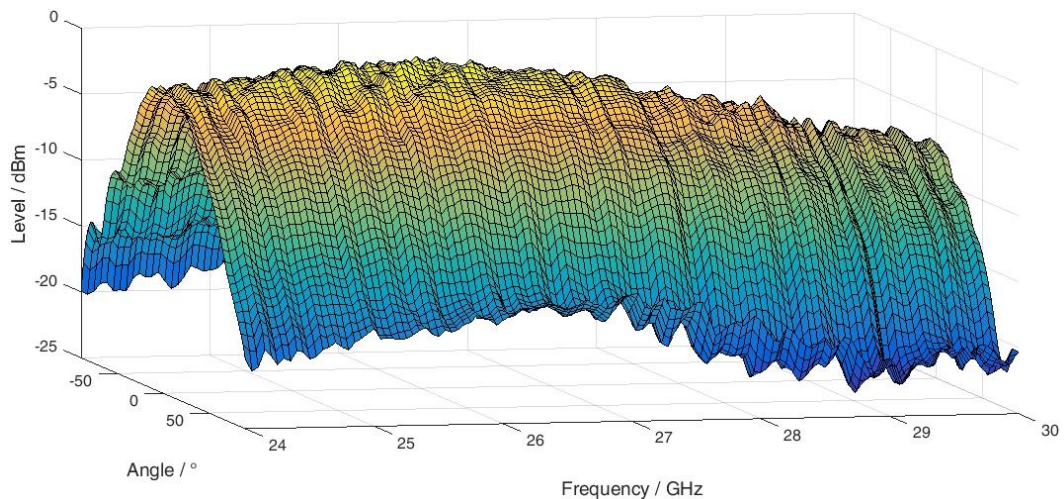


Figure 17: 2D-Swept Radiation Pattern of one Element

5.1.2 Simulation Results based on measured single Element Patterns

As introduced by equation (5) in chapter 4.1, the radiation pattern of a linear array can be calculated by multiplying a single measured element radiation pattern F_{element} with the array factor AF_{array} .

All figures in chapter 4.3 were simulated using omnidirectional antenna elements and the actual dimensions of the linear array whose element radiation patterns are shown in Figure 15 and Figure 17. Using a single measured element radiation pattern as F_{element} instead of omnidirectional data helps to increase the accuracy of the simulated pattern calculated with equation (5).

Figure 18 and Figure 19 illustrate the difference between assuming an omnidirectional radiation characteristic and using actual measured data of one element. A closer look at the figures reveals an increased boresight gain for the simulation using measured data due to the non-omnidirectional characteristic of the elements.

For the simulation, all antenna gains were set to 0 dBi and the element spacing was fixed at 16 mm in free space.

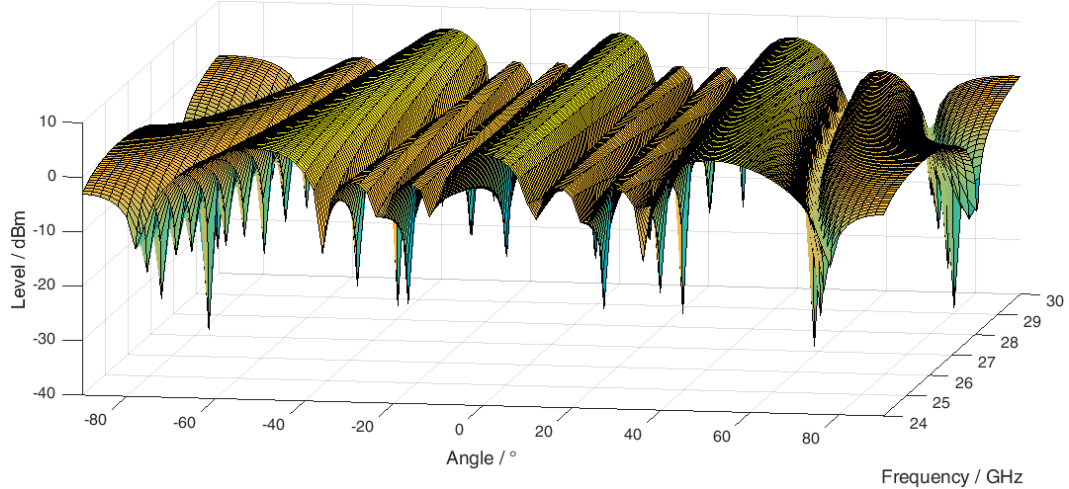


Figure 18: Simulation with isotropic Elements

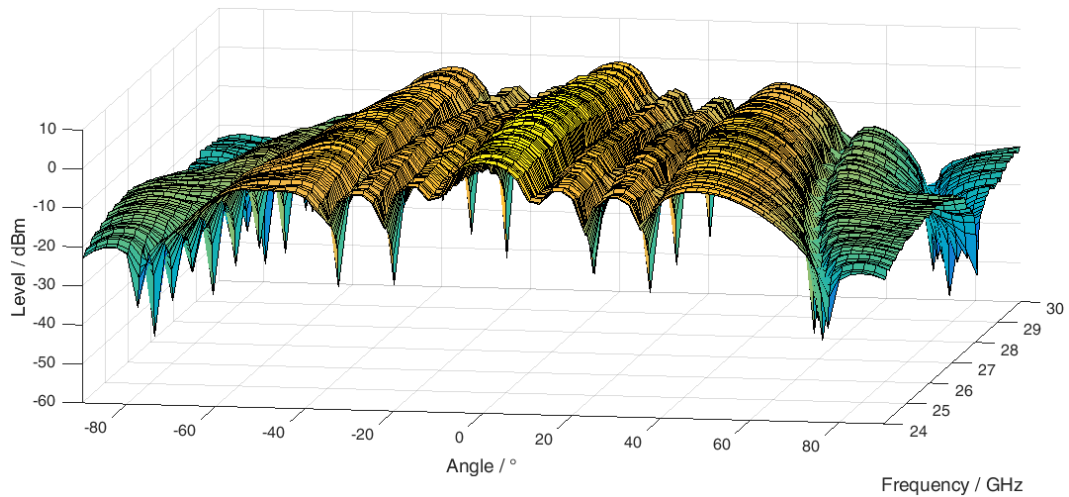


Figure 19: Simulation using a single measured Element Radiation Pattern

Combining equation (3) and (6) provides means to steer an antenna beam to arbitrary directions. The effects on the radiation pattern vary depending on the desired angle. As the beam is steered further away from boresight, the main lobe gets more and more attenuated while its width increases.

Figure 20 shows these effects for 26 GHz and 28 GHz. The two patterns are the result from using the measured element pattern (red) and assuming an omnidirectional characteristic (blue) for the calculations. The yellow vertical line indicates the intended beam steering direction.

Without any phase difference between the elements, the boresight gain of the measured elements results in an increased main lobe level in comparison to the side lobes. Increasing the beam steering angle significantly decreases the amplitude of the main lobe.

While there is no amplitude difference for the lobes of the array using perfectly omnidirectional elements, the level of the main lobe is maintained over all angles due to the isotropic radiators.

Both simulated radiation patterns suffer from an increasing beam width when steered to larger angles.

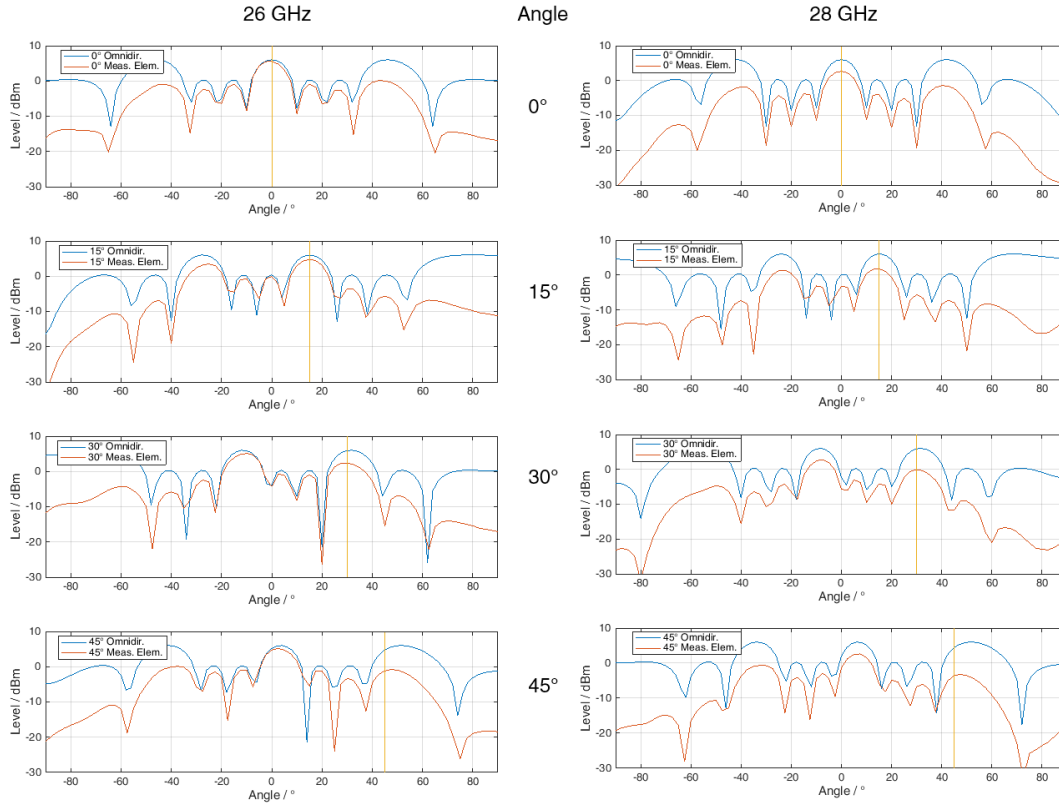


Figure 20: Beamsteering at different Frequencies

5.2 Antenna Scan

Figure 21 shows the result of a frequency sweep using the linear antenna array over a range of 2 GHz. The measurement was made using an R&S®ZVA network analyzer equipped with four independent sources. This instrument provides phase coherent signal output comparable to a digital beamforming architecture as introduced in chapter 3.2. The setup used for these measurements is described in [5].

A direct comparison to the simulated pattern of an antenna array with the same geometry using the measured element data is given by Figure 22. Overall the measurement is in line with the simulation. Beam width and distance between the main and side lobes match for both results.

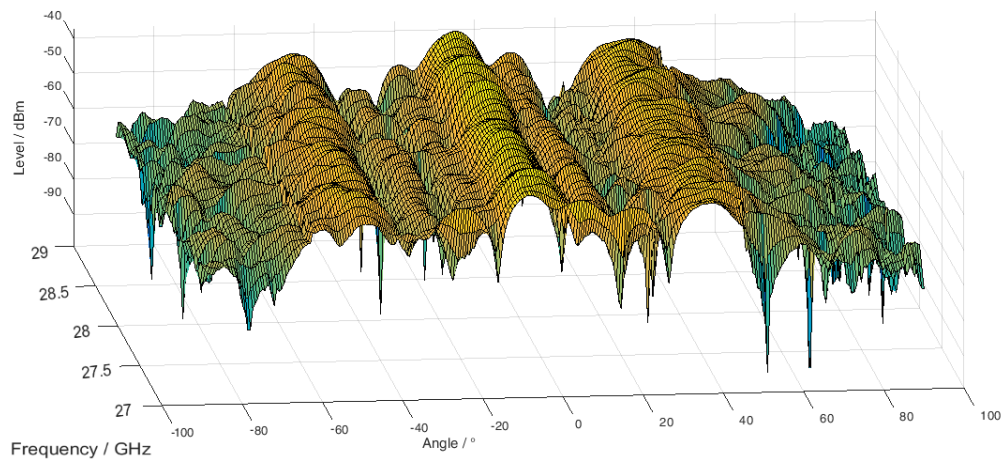


Figure 21: Measured Frequency Scan

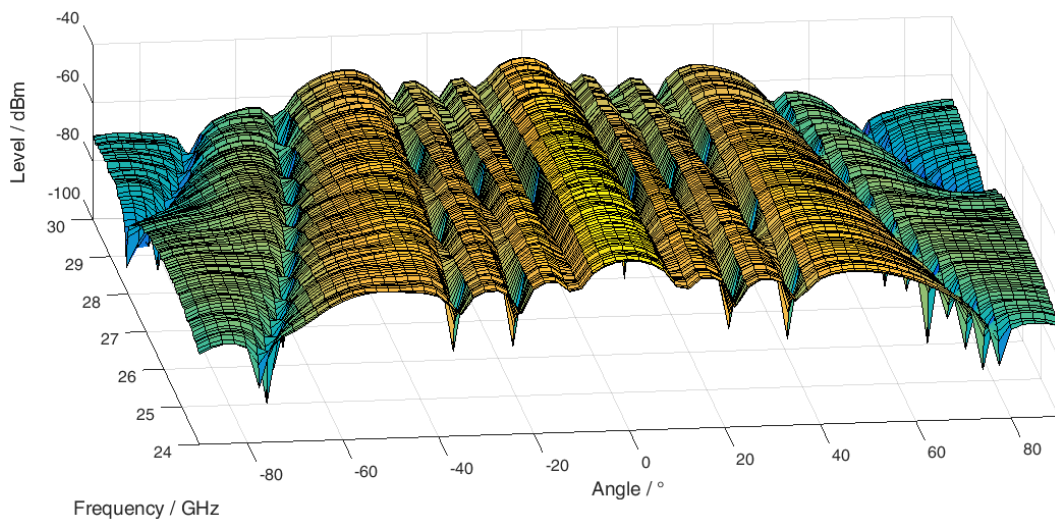


Figure 22: Simulated Frequency Scan

5.3 Further reading

This section illustrated uniform linear arrays as defined in the introduction. Apart from budget, the permissible physical size, target band, user application and physical surroundings for the array determines if a more complex arrangement is feasible.

An introduction to the use of planar arrays, conducted measurements as well as the choice of waveform properties for steering array antennas is given in reference [17].

6 Results and Outlook

It is already widely accepted that beamforming will play an important role in the implementation of next generation networks. Many 5G topics are still subjects of ongoing research, but the general direction taken by the industry includes small as well as large beamforming arrays, the latter in part only made feasible by the shorter wavelengths encountered in millimeter-wave bands.

This paper introduced some aspects of beamforming technology from basic signal propagation to the implementation of a small uniform linear array architecture.

Rohde & Schwarz continues to optimize 5G test solutions for this and other techniques currently being considered for the 5th Generation in cellular wireless communication.

7 Appendix

7.1 MATLAB® Pattern Generation Script

These MATLAB®¹ code excerpts provide functions to generate radiation pattern similar to those shown in chapter 4.3.

The *main* function makes use of the two auxiliary functions:

LinearArrayFactor_EIwise for calculating the frequency dependent array factor depending on the number of elements and complex weights

Friis_Equation returns the free field attenuation depending on the setup and frequency used.

7.1.1 Main Function

```
%% Constants
freq_range = [24 28];           % [start_frequency stop_frequency] /
GHz
freq_points = 100;             % No. of frequency points
d = 16;                        % Element spacing / mm
N = 4;                          % Number of elements
amp_weights = [1 1 1 1];      % Amplitude weights for N elements
from 0 to 1
phase_delta = [0 0 0 0];      % Phase weights for N elements / deg
gain_trans = 0;                % Gain of transmission antenna / dBi
gain_rec = 0;                  % Gain of receive antenna / dBi
trans_power = 0;               % Transmitted power / dBm
send_dist = 5;                 % Distance of Transmission / m

%% create frequency and angle vector for simulation data
freq_step = (freq_range(2)-freq_range(1))/freq_points;
vFrequency = freq_range(1):freq_step:freq_range(2)+freq_step;
vAngle = -90:1:90;
deg2rad = pi/180;
vTheta_rad = vAngle * deg2rad;
```

¹ MATLAB™ is a registered trademark of The Mathworks Inc.

```

%% go through whole bandwidth and calculate the radiation pattern
currfreq = freq_range(1); ii = 1;
while (currfreq <= freq_range(2))
    % create omnidirectional characteristic
    iPattern = zeros(1,length(vAngle));

    % Calculate Array Factor
    [AF, ~] = LinearArrayFactor_ElWise(vTheta_rad(:)',
currfreq*1e9, d, N, amp_weights, phase_delta.*deg2rad);
    F = 10*log10(AF) + iPattern;
    F_real(ii,:) = real(F(:));

    % increment counter
    ii = ii +1;
    currfreq = vFrequency(ii);
end

%% Plot
figure;
surf(vAngle,vFrequency(1:end-1),F_real);
ax = gca;
ax.YAxis.TickLabelFormat = '%,.1g';
set(ax, 'FontSize',12)
rotate3d on;
xlim([-90 90]);
ylabel('\fontsize{14}Frequency / GHz');
xlabel('\fontsize{14}Angle / °');
zlabel('\fontsize{14}Level / dBm');

```

7.1.2 Linear Array Factor Function

```

function [AF, AF_dB] = LinearArrayFactor_ElWise (vTheta_rad, f, d,
N, weights, phaseDiff)

%ArrayFactor Calculate array factor of linear antenna array based
on

%frequency f [Hz], element spacing d [mm], number of elements N
and phase shift between elements beta [rad] theta in rad as well

% global constants
c = 299792458;

% calculate array factor
lambda = c / f;
k      = 2 * pi / lambda;
phi    = (k * d/1e3 * sin(vTheta_rad));

AF = zeros(1, length(vTheta_rad));
for ii = 1:N
    AF = AF + weights(ii).*exp(1i*phi*ii).*exp(-1i*phaseDiff(ii));
end
AF_dB = 20*log10(AF);
end

```

8 References

- [1] V. Rabinovich and N. Alexandrov, *Antenna Arrays and Automotive Applications*: Springer, 2013, pp. 24-52.
- [2] A. Roessler, "5G Waveform Candidates," Rohde & Schwarz GmbH & Co. KG, München, 2016.
- [3] T. Braunstorfinger, "Phase Adjustment of Two MIMO Signal Sources with Option B90 (Phase Coherence)," Rohde & Schwarz GmbH & Co. KG, München, 2009.
- [4] C. Tröster-Schmid and T. Bednorz, "Generating Multiple Phase Coherent Signals – Aligned in Phase and Time," Rohde & Schwarz GmbH & Co. KG, München, 2016.
- [5] M. Naseef, G. Lloyd, and M. Reil, "Characterizing Active Phased Array Antennas," Rohde & Schwarz GmbH & Co. KG, München, 2016.
- [6] ITU-R, Ed., "Attenuation by atmospheric gases: ITU-R P.676-10," 2013.
- [7] J. Butler and R. Lowe, "Beamforming matrix simplifies design of electronically scanned antennas," 1961.
- [8] C. Powell, "Technical Analysis: Beamforming vs. MIMO Antennas," 2014.
- [9] A. Alkhateeb, J. Mo, N. González-Prelcic, and Heath, Robert W. Jr., "MIMO Precoding and Combining Solutions for Millimeter-Wave Systems," IEEE, 2014.
- [10] R. Wonil *et al.*, "Millimeter-Wave Beamforming as an Enabling Technology for 5G Cellular Communications: Theoretical Feasibility and Prototype Results," IEEE 52, 2014.
- [11] X. Gu *et al.*, "W-Band Scalable Phased Arrays for Imaging and Communications," IEEE 53, 2015.
- [12] M. I. Skolnik, *Introduction To Radar Systems*: Mcgraw Hill Book Co, 1961, pp. 280-286.
- [13] K. S. Das and A. Das, *Antenna and Wave Propagation*: Tata McGraw Hill Education Private Limited, 2013, pp. 153-163.
- [14] I. V. Minin and Minin Oleg V., *Basic Principles of Fresnel Antenna Arrays*: Springer Science & Business Media, 2008, p. 12.
- [15] S. I. Nikolov and H. Jensen, "Manipulation of Grating Lobes by Changing Element Shape," 34, 2011.
- [16] B. Allen and M. Ghavami, *Adaptive Array Systems: Fundamentals and Applications*: John Wiley & Sons, 2006, pp. 44 - 52.
- [17] M. Kottkamp and C. Rowell, "Antenna Array Testing - Conducted and Over the Air: The Way to 5G," München, 2016.

Rohde & Schwarz

The Rohde & Schwarz electronics group offers innovative solutions in the following business fields: test and measurement, broadcast and media, secure communications, cybersecurity, radiomonitoring and radiolocation. Founded more than 80 years ago, this independent company has an extensive sales and service network and is present in more than 70 countries.

The electronics group is among the world market leaders in its established business fields. The company is headquartered in Munich, Germany. It also has regional headquarters in Singapore and Columbia, Maryland, USA, to manage its operations in these regions.

Regional contact

Europe, Africa, Middle East
+49 89 4129 12345
customersupport@rohde-schwarz.com

North America
1 888 TEST RSA (1 888 837 87 72)
customer.support@rsa.rohde-schwarz.com

Latin America
+1 410 910 79 88
customersupport.la@rohde-schwarz.com

Asia Pacific
+65 65 13 04 88
customersupport.asia@rohde-schwarz.com

China
+86 800 810 82 28 | +86 400 650 58 96
customersupport.china@rohde-schwarz.com

Sustainable product design

- Environmental compatibility and eco-footprint
- Energy efficiency and low emissions
- Longevity and optimized total cost of ownership



This and the supplied programs may only be used subject to the conditions of use set forth in the download area of the Rohde & Schwarz website.

R&S® is a registered trademark of Rohde & Schwarz GmbH & Co. KG; Trade names are trademarks of the owners.